Frictional strengths of talc-serpentine and talc-quartz mixtures

Diane E. Moore[1] and David A. Lockner[1]

Received 22 July 2010; revised 4 October 2010; accepted 1 November 2010; published 15 January 2011.

[1] Talc is a constituent of faults in a variety of settings, and it may be an effective weakening agent depending on its abundance and distribution within a fault. We conducted frictional strength experiments under hydrothermal conditions to determine the effect of talc on the strengths of synthetic gouges of lizardite and antigorite serpentinites and of quartz. Small amounts of talc weaken serpentinite gouges substantially more than predicted by simple weight averaging. In comparison, mixtures of quartz and talc show a linear trend of strength reduction at talc concentrations ≤15 wt % and enhanced weakening at higher concentrations. All of the strength data are fit by a modified version of the Reuss mixing law that allows for the dominance of one mineral over the other. The difference in the behavior of serpentinite-talc and quartz-talc mixtures at low talc concentrations is a reflection of their different textures. Lizardite, antigorite, and talc all have platy habits, and displacement within gouges composed of these minerals is localized to narrow shears along which the platy grains have rotated into alignment with the shear surfaces. The shears in the mixed phyllosilicate gouges maximize the proportion of the weaker mineral within them. When mixed with a strong, rounded mineral such as quartz, some minimum concentration of talc is needed to form connected pathways that enhance strength reductions. The typical development of talc by the reaction of Si-rich fluids with serpentinite or dolomite would tend to localize its occurrence in a natural fault and result in enhanced weakening.

Citation: Moore, D. E., and D. A. Lockner (2011), Frictional strengths of talc-serpentine and talc-quartz mixtures, *J. Geophys. Res.*, *116*, B01403, doi:10.1029/2010JB007881.

1. Introduction

[2] The sheet-silicate mineral talc is stable at physical conditions that range from the surficial environment to temperatures of 700°C–800°C and pressures as high as ≈5 GPa [*Chernosky et al.*, 1985; *Jenkins et al.*, 1991; *Pawley and Wood*, 1995]. Because of its high magnesium content, talc is a common constituent of ultramafic rocks, which figure importantly in a variety of plate boundary settings. Talc has been reported in exhumed subduction zone thrust faults [e.g., *Peacock*, 1987; *Bebout and Barton*, 2002; *King et al.*, 2003] and oceanic fracture zones and detachment faults associated with rift systems [*Boschi et al.*, 2006]. In addition, small amounts of talc have been found in serpentinite in the central creeping section of the San Andreas fault [*Moore and Rymer*, 2007], a continental plate boundary transform fault. Talc is not limited in its occurrence to ultramafic rocks; for example, it has been found in exhumed, low-angle normal faults in Italy, where it was the product of silica metasomatism of dolomite [*Collettini et al.*, 2009b; *Viti and Collettini*, 2009]. Talc potentially could have a significant impact on the mechanical properties of faults in these various settings because it is extremely weak and is characterized by velocity-strengthening behavior that would tend to stabilize slip [*Moore and Lockner*, 2004, 2008].

[3] The amount of talc present in these faults varies widely. In one occurrence, a 4 m thick zone along an exhumed subduction thrust in the Trinity Alps of California is antigorite serpentinite that contains about 30 modal % talc on average and as much as 75% talc locally [*Peacock*, 1987]. Similarly, tectonic blocks of serpentinized ultramafic rock in Franciscan mélange at Cape San Martin, California, are interpreted by *King et al.* [2003] to preserve metasomatic zones developed in the mantle wedge during subduction. One of the metasomatic zones replacing antigorite serpentinite at Cape San Martin is as much as 20 m thick and contains 85–90 modal % talc. The frictional properties of these and similarly talc-rich faults should be dominated by the weak talc. At the other extreme, the trace amounts of talc identified thus far in cuttings of serpentinite from the San Andreas Fault Observatory at Depth (SAFOD) drill hole [*Moore and Rymer*, 2007] might have little influence on fault strength. This raises the question of how much talc is needed to significantly weaken a fault.

[4] Room temperature friction experiments conducted on mixtures of quartz and clay minerals yield weakening trends that vary with the type of clay mineral tested. Quartz-kaolinite [*Crawford et al.*, 2008] and quartz-illite [*Tembe et al.*, 2010] follow a roughly linear trend of strength reduction with increasing clay content. In contrast, montmorillonite

[1]U.S. Geological Survey, Menlo Park, California, USA.

concentrations above ≈15 wt % in a quartzose gouge weaken the gouge to a greater degree than that predicted from a linear strength-composition relation [e.g., *Tembe et al.*, 2010]. The frictional strength of talc is comparable to that of montmorillonite and the two minerals might be expected to have a similar effect on quartz gouge strength. To date, however, little attention has been paid to mixtures of sheet-silicate minerals that have different strengths, such as talc and serpentine [*Van Diggelen et al.*, 2009]. A shear zone developed in a gouge that is rich in sheet-silicate minerals (with their typically platy habits) has a different texture from one formed in a gouge consisting largely of grains with rounded to subangular shapes. A weak, platy mineral such as talc might be incorporated in different ways into these different types of shears.

[5] To address these questions, we conducted triaxial tests on mixtures of talc with lizardite-rich and antigorite-rich serpentinites and with quartz, using a saw cut shear assembly. The experiments were run at elevated temperatures and effective pressures to approximate the conditions found at depth within a fault zone (roughly 6–14 km depth for crustal faults). We find that even minor amounts of talc substantially weaken the serpentinite gouges, whereas the effect of talc on quartz gouges is similar to that of montmorillonite on quartz at high effective stress, as predicted. In addition, a small amount of talc localized in its occurrence in a serpentinite gouge has a weakening effect equal to that of a uniformly mixed gouge with an order of magnitude higher talc concentration. Thus, even very minor amounts of talc can have a major influence on fault strength, if concentrated along fractures or shears.

2. Experiments Conducted

2.1. Starting Materials

[6] The sheet-silicate gouges used in these experiments are from the same stocks prepared for previous studies [e.g., *Moore et al.*, 1997; *Moore and Lockner*, 2007, 2008]. The talc gouge is a mineral separate made from coarse-grained, talc-rich schists from Balmat, New York (obtained from Wards Natural Science); it is monomineralic, as determined by powder X-ray diffraction (XRD) analysis. The lizardite gouge comes from a thoroughly serpentinized peridotite from Gold Beach, Oregon (collected by R. G. Coleman), that consists of >90% serpentine, nearly all lizardite, with magnetite as the principal accessory mineral [*Moore et al.*, 1996]. The antigorite-serpentinite gouge is derived from a block collected at the KCAC asbestos mine near New Idria, California. It contains ≈75% serpentine, of which antigorite is the only serpentine variety identified in the bulk powder XRD patterns. Magnetite is also the major accessory mineral in this gouge, along with some calcite and chlorite. Although impure, the frictional strength of the New Idria antigorite-rich gouge is the same as that of a monomineralic antigorite gouge [*Morrow et al.*, 2000; *Moore and Lockner*, 2007]. Preparation of the serpentinite samples was limited to the removal of veins and altered-looking areas. Each sheet-silicate sample was manually ground and passed through a 90 μm sieve.

[7] The quartz gouge is from the same quartz stock that was used by *Tembe et al.* [2010] for room temperature friction experiments on mixtures of quartz and clay minerals. It is a commercially acquired Ottawa sand (>99% quartz) that was crushed and sieved to <180 μm grain size.

2.2. Procedures

[8] We ran three series of triaxial experiments (Table 1) at elevated temperatures, using the saw cut sample configuration plus furnace assembly illustrated in Figure 1. Temperatures (T) were chosen to be consistent with the stability ranges of the minerals being tested. Lizardite is the dominant low-temperature serpentine mineral, and antigorite is the high-temperature (300°C $\leq T \leq$ ~600°C) variety. Accordingly, we ran the lizardite-talc series at 200°C and the antigorite-talc series at 400°C. Two additional experiments were conducted on 50:50 mixtures of lizardite-talc and antigorite-talc at 300°C to link the two series. The quartz-talc series was conducted at 200°C. All of the experiments were run at a constant effective normal stress, σ_N, of 100 MPa (50 MPa fluid pressure of deionized water and 150 MPa normal stress, roughly corresponding to hydrostatic fluid pressures).

[9] Each sample consisted of a layer of gouge housed between driving blocks that were prepared by cutting a rock cylinder 19.1 mm in diameter and 41 mm in length into two pieces at a 30° angle to the cylinder axis (Figure 1). Rock types for the driving blocks were chosen to be chemically compatible with the gouge mixtures. The two series involving serpentine minerals used cylinders of dunite for the forcing blocks, and the quartz-talc series used Westerly granite cylinders (Table 1). The saw cut surfaces were ground with 120 grit SiC. Mixtures by weight were prepared from portions of the end-member gouges that had been dried in a vacuum oven at 120°C for a few hours. For all but one experiment, an initial 1 mm thick layer of gouge was smeared as a thick paste onto the lower driving block, and the upper block was then placed on top of the gouge layer. The single "sandwich" sample (Table 1) consisted of two 1 mm thick layers of the lizardite gouge, one applied to each saw cut surface, with a small quantity of talc sprinkled on the surface of one layer before the two pieces were placed together. The talc comprised roughly 2 wt % of the gouge in the sandwich sample, as estimated by weighing the room dry gouge stocks before and after sample preparation.

[10] The upper driving block contained a throughgoing, 2.5 mm diameter borehole for pore fluid entry; a hollow steel tube (2.35 mm outer diameter, 0.8 mm diameter opening at the base and 1.5 mm opening at the top) inserted into the borehole during sample assembly minimized the extrusion of gouge into the opening. The gouge-filled cylinder was placed in a jacket between titanium carbide end plugs and alumina insulators. The narrow space between the jacket and the furnace wall was loosely packed with boron nitride, which is a good thermal and poor electrical conductor. Once in the pressure vessel, confining pressure (argon gas) was first increased to 70–80 MPa, while the pore pressure lines were evacuated. After fluid pressure of 50 MPa was applied, confining pressure was raised to the starting value of 150 MPa as the sample was heated. Temperature was monitored by a thermocouple inserted along the pore pressure inlet to the top of the sample. The samples were centered at the temperature maximum in the furnace; temperature varied by ≈1% along the length of the gouge layer. Axial displacement rates ranged between 0.01 and 1.0 μm/s;

Table 1. Summary of Friction Experiments

Gouge Composition (wt % Talc)	T(°C)	Forcing Blocks
Lizardite-Talc Series		
0	200	dunite
≈2 (sandwich)	200	dunite
5	200	dunite
10	200	dunite
25	200	dunite
50	200	dunite
75	200	dunite
100[a]	200	serpentinite
50	300	dunite
Antigorite-Talc Series		
50	300	dunite
0[b]	400	dunite
5	400	dunite
10	400	dunite
25	400	dunite
50	400	dunite
75	400	dunite
100[a,c]	400	serpentinite
Quartz-Talc Series		
0	200	granodiorite
5	200	granodiorite
10	200	granodiorite
15	200	granodiorite
25	200	granodiorite
50	200	granodiorite
75	200	granodiorite
100	200	granodiorite

[a]*Moore and Lockner* [2007, 2008].
[b]*Moore and Lockner* [2007].
[c]Run at ≈111 MPa σ_N.

corresponding displacement rates along the inclined saw cut are ≈0.0115 and ≈1.15 μm/s, respectively. Constant normal stress during an experiment was maintained by means of computer-controlled adjustments to the confining pressure.

[11] The absolute value of seal friction was subtracted from the load-cell reading before sample contact. Because seal friction is a function of confining pressure, an additional correction was applied during the experiment to account for the continuing adjustments to confining pressure to maintain a constant normal stress. The velocity dependence of seal friction was checked at the beginning of each experiment by means of a velocity step that was made before the piston touched the sample. Corrections for changes in contact area along the sliding surface were made during the experiment as described by *Scott et al.* [1994] and *Tembe et al.* [2010]. A greased Teflon shim was placed between the sample and forcing piston (Figure 1) to allow for lateral slip of the lower driving block during shear. The correction to the normal stress for lateral slip on the Teflon shim is +0.7 MPa (see *Tembe et al.* [2010] for more detailed discussion of this correction).

[12] The shear resistance of the jacket is removed from the total shear stress after the experiment. Copper and lead jackets, with different strength profiles, were used in this study. Corrections for the Cu jackets, which were used for the serpentine-talc experiments, are described by *Moore and Lockner* [2008]. A method for preparing uniformly thin-walled (0.5 mm wall thickness) Pb jackets with few imperfections was developed by Lockner during the course of this study. Because of its low strength and high ductility, Pb is an excellent jacketing material for low-temperature experiments (T < 250°C), and the quartz-talc series was run with Pb jackets prepared by the new process. Lead jackets with 1.0 mm wall thickness used in earlier calibration experiments were determined to have a yield stress of 1.8 MPa at room temperature [*Moore and Lockner*, 2008]. Consistent with that, the 0.5 mm jackets were found to have a yield stress of 0.9 MPa at room temperature. The yield stress decreases linearly to 0 at ≈250°C, and there is no strain-hardening term. The correction to the shear stress of the quartz-talc experiments at 200°C is a nominal 0.2 MPa. Because the coefficient of friction is the ratio of shear to effective normal stress, systematic errors due to seal friction, stress calibrations, and sample contact area partially cancel in computing this ratio. We estimate that typical uncertainties in determining coefficient of friction range from approximately ±0.02 for Pb jacket tests to ±0.03 for Cu jacket tests run at 200°C.

[13] Thin sections were prepared from several of the tested samples for examination with a petrographic microscope. To prepare the thin sections, the jacketed samples were impregnated with epoxy resin before being sliced along the length of the cylinder and perpendicular to the saw cut. The jackets were removed from several other samples for preliminary examination with a stereomicroscope, after which small, oriented fragments of gouge were mounted on

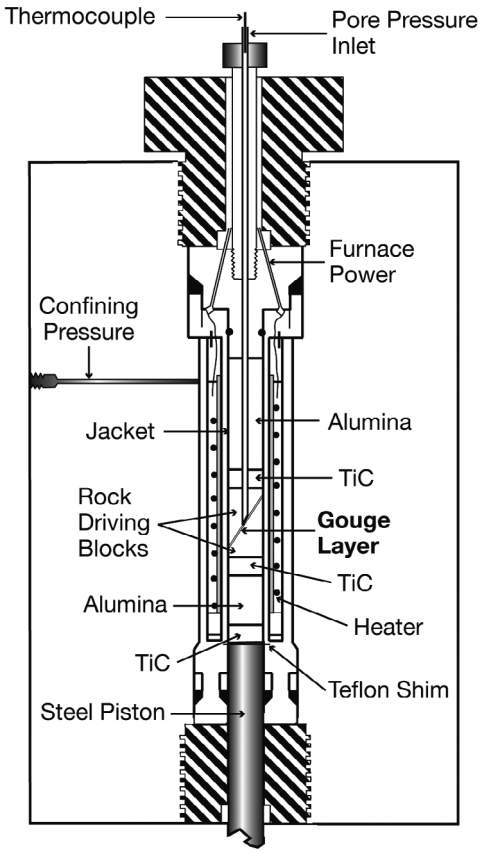

Figure 1. Experimental assembly.

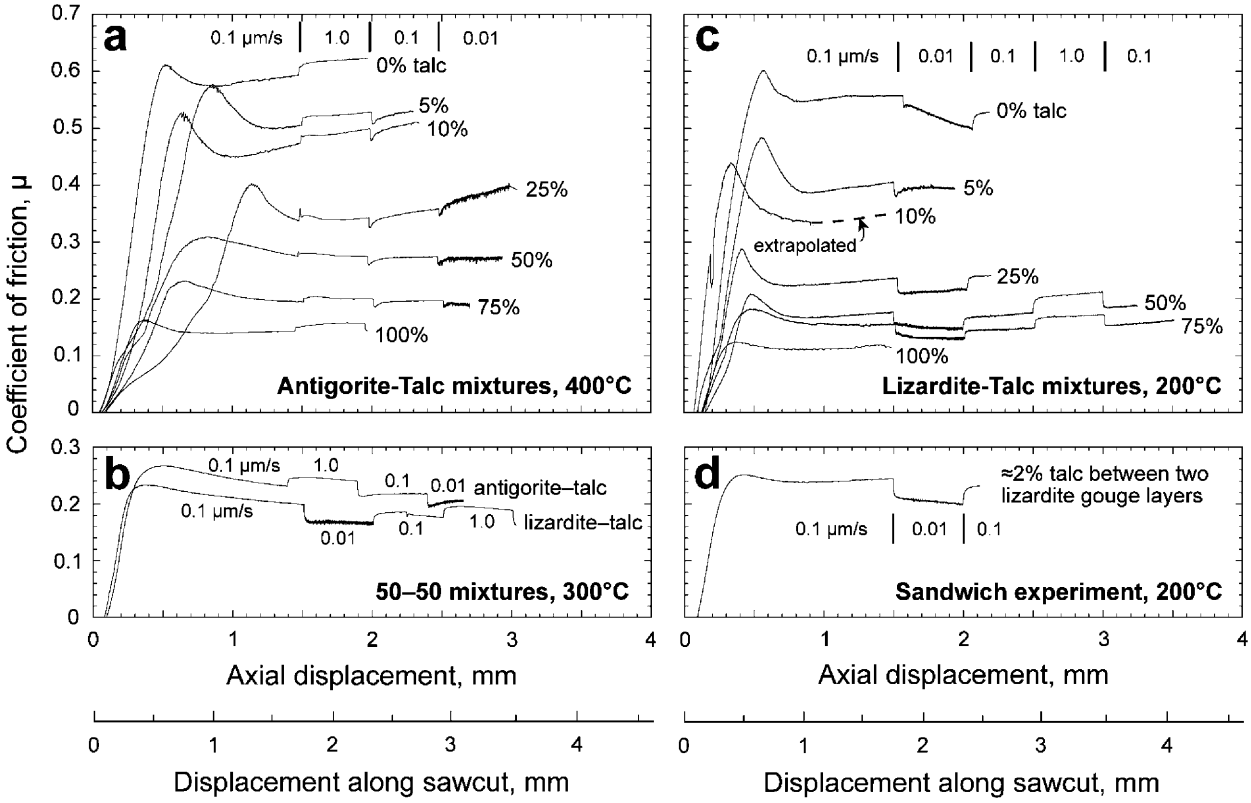

Figure 2. Frictional strength experiments on mixtures of serpentine and talc. All experiments were run at 50 MPa pore pressure and 150 MPa normal stress (100 MPa σ_N). (a) Antigorite-talc series at 400°C. The sequence of velocity steps, reported as axial velocities, is shown at the top. Irregular initial behavior (0–1 mm axial displacement) of the 25% talc sample was probably caused by a slight misalignment of the sample in the jacket during assembly. (b) Equal mixtures by weight of antigorite and talc and of lizardite and talc, run at 300°C. (c) Lizardite-talc series at 200°C. Data for the experiment on 100% talc [*Moore and Lockner*, 2007, 2008] at >1.5 mm displacement are omitted here, because the second velocity step was 1 μm/s (see Figure 10 for the entire plot). (d) Lizardite-talc "sandwich" experiment at 200°C.

plugs for petrographic analysis with a scanning electron microscope (SEM).

3. Results

3.1. Strength Data

[14] Strength-displacement plots for all experiments are presented in Figures 2 and 3. The order of the velocity steps at 1.0 and 0.01 μm/s was reversed in different series. The 1.0 μm/s step had come first for the previous 400°C experiments on the antigorite and talc end-members (Table 1), and the rest of the antigorite-talc series was conducted in the same order (Figures 2a and 2b). The 0.01 μm/s rate came first in the lizardite-talc (Figures 2b–2d) and quartz-talc (Figure 3) series.

[15] Under water-saturated conditions, the serpentine minerals lizardite and antigorite are not as strong as quartz or other "Byerlee's rule" minerals, but they are among the stronger sheet silicates [*Morrow et al.*, 2000; *Moore and Lockner*, 2004]. The two serpentine minerals have similar strengths that increase somewhat with increasing temperature [*Moore et al.*, 1997; *Moore and Lockner*, 2007]. At 400°C the antigorite gouge has a coefficient of friction, $\mu \approx 0.6$ (Figure 2a), and $\mu \geq 0.5$ at 200°C for the lizardite gouge (Figure 2c), consistent with previous results for lizardite at similar conditions [*Moore et al.*, 1997]. Talc is somewhat stronger at 400°C ($\mu \sim 0.14$–0.16) than at 200°C ($\mu \sim 0.12$–0.13) (Figures 2a and 2c), but both values are lower than its room temperature strength ($\mu \sim 0.18$ at 100 MPa σ_N) [*Moore and Lockner*, 2008].

[16] All of the mixtures of serpentine and talc have strengths intermediate between their respective end-members, but strength does not vary linearly with composition. Considering first the antigorite-talc series (Figure 2a), adding 5 wt % talc to the antigorite gouge leads to a reduction in μ of 0.09, which is nearly one-fifth the difference in strength between the end-members. The strength of the 25 wt % talc sample is roughly midway between the strengths of the end-member gouges. The 50:50 mixture is slightly weaker at 300°C than at 400°C (Figures 2a and 2b). In each experiment, the strength of the gouge increases initially to a peak and then drops to a residual value. Strength-displacement plots for the samples containing 0–25 wt % talc have sharper peaks than those containing 50–100 wt % talc. Samples containing 0–25 wt % talc also strain harden somewhat with continued shear, whereas those containing 50–100% talc do not strain harden. Because of

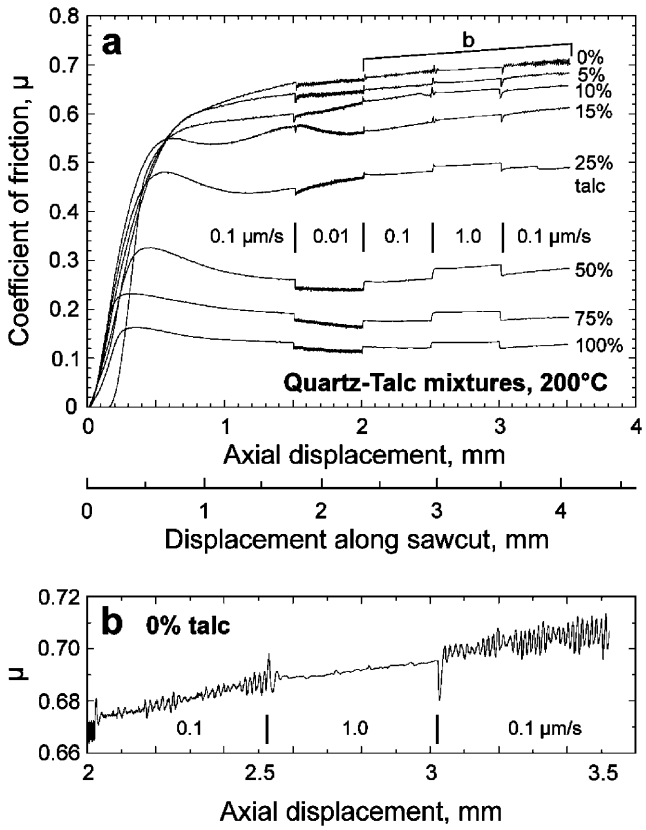

Figure 3. (a) Frictional strength experiments on mixtures of quartz and talc at 200°C. A clogged bleed valve caused normal stress to increase at the beginning of the 10% talc experiment. The experiment was restarted after the problem was fixed, but the zero position was slightly offset. (b) Blowup of part of the curve for the pure quartz sample (0% talc), which is characterized by intermittent periods of unstable slip during the 0.1 μm/s steps.

premature jacket failures, data are lacking for several velocity steps. In most cases, an increase in sliding velocity leads either to no change or to a slight increase in μ. However, in the 25 wt % talc experiment μ is slightly lower during the 0.1 μm/s step than for the subsequent step at 0.01 μm/s. Quantitative consideration of the effects of changing velocity is presented in the next section.

[17] Talc has a very pronounced weakening effect on the lizardite gouge at 200°C (Figure 2c). Adding only 5 wt % talc to lizardite lowers μ to ≈0.4. The strength of the 25% talc sample is reduced by about 75% of the difference between the lizardite and talc end-members, as is the sandwich sample containing ~2% talc (Figure 2d). Similar to the antigorite-talc series, those mixtures containing more lizardite than talc generally have a sharper initial peak in strength, although the strength plot for the sandwich sample with 2 wt % talc resembles the talc-rich mixtures. The coefficient of friction is consistently higher at the faster velocity for the lizardite-talc series.

[18] The talc gouge tested in the lead jacket at 200°C (Figure 3) has the same strength as the talc sample tested in the equivalent experiment using a Cu jacket (Figure 2c). For the quartz gouge $\mu \approx 0.7$, consistent with other experimental data reported for quartz at elevated temperatures [e.g., *Higgs*, 1981; *Chester and Higgs*, 1992]. The quartz gouge displayed intermittent periods of unstable behavior at 0.1 μm/s (Figures 3a and 3b), although these strength oscillations remain quasi-stable. Adding small amounts of talc to the quartz gouge causes μ to decrease, but by relatively small amounts compared to equivalent serpentinite-talc mixtures. The most pronounced reduction in quartzose-gouge strength occurs between 15 and 50% talc. The strength plots for samples containing 15–100% talc show an initial peak similar to those for the talc-rich samples in Figure 2. For gouge layers containing 0–10% talc, the rapid initial rise in strength gives way to a modest strain hardening thereafter. Between 2 and 3.5 mm axial displacement, the 15–50% talc samples also strain harden slightly, whereas μ levels off for the gouges containing 75 and 100% talc. There is little change in μ with changing velocity for the samples with 0–15% talc, whereas for those containing 50–100% talc μ is consistently higher at the faster velocity. The 25% talc sample is transitional between these two groups.

[19] The variations in μ with gouge composition at a given displacement are compared in Figure 4. Data for the two serpentine-talc series represent the end of the initial 0.1 μm/s velocity step at ≈1.5 mm axial displacement (Figure 4a). One experiment (10% talc, Figure 2c) that failed at ≈0.9 mm displacement was extrapolated to 1.5 mm consistent with the trends of the samples with 5 and 25% talc. For the quartz-talc series (Figure 4b), the values of μ at 1.5 and 3.5 mm are presented. Because of the inclined saw cut geometry, corresponding fault-parallel displacements are approximately 1.7 and 4.0 mm, respectively.

[20] Figure 4a highlights the marked effect of even small amounts of talc on serpentinite gouge strength. There is a significant drop in strength between 0 and 25% talc, and a more gradual decrease at higher talc concentrations. The 300°C data for the 50:50 mixtures plot between the two trends. The sandwich sample, containing a thin concentrated layer of talc, has strength similar to the mixture of 25% talc and 75% lizardite. The values of μ at the two displacements for the quartz-talc series (Figure 4b) illustrate the differences in strain-hardening behavior described previously. Mixtures containing 0–50% talc have higher values of μ at 3.5 mm, whereas μ is essentially constant for the samples with 75 and 100% talc. At 3.5 mm displacement, the gouges containing ≤15 wt % talc fall on a straight line connecting the end-members, whereas the rest of the mixtures follow a curved trend below the line. The data set at 1.5 mm is shifted to slightly lower values of μ on the quartz-rich side, but retains the linear trend between 0 and 15% talc.

3.2. Velocity Dependence of Strength

[21] The sliding rate sensitivity of shear strength is represented by the change in steady state coefficient of friction, $\Delta\mu_{ss}$, resulting from a logarithmic change in velocity, V: $\Delta\mu_{ss}/\Delta\ln V$. In these experiments, 0.1 μm/s was used as a reference velocity, such that the axial velocity alternated between that and the other two rates. This procedure helped to separate velocity-dependent from displacement-dependent changes in frictional resistance. For each velocity step, the change in μ was measured, along with error estimates that

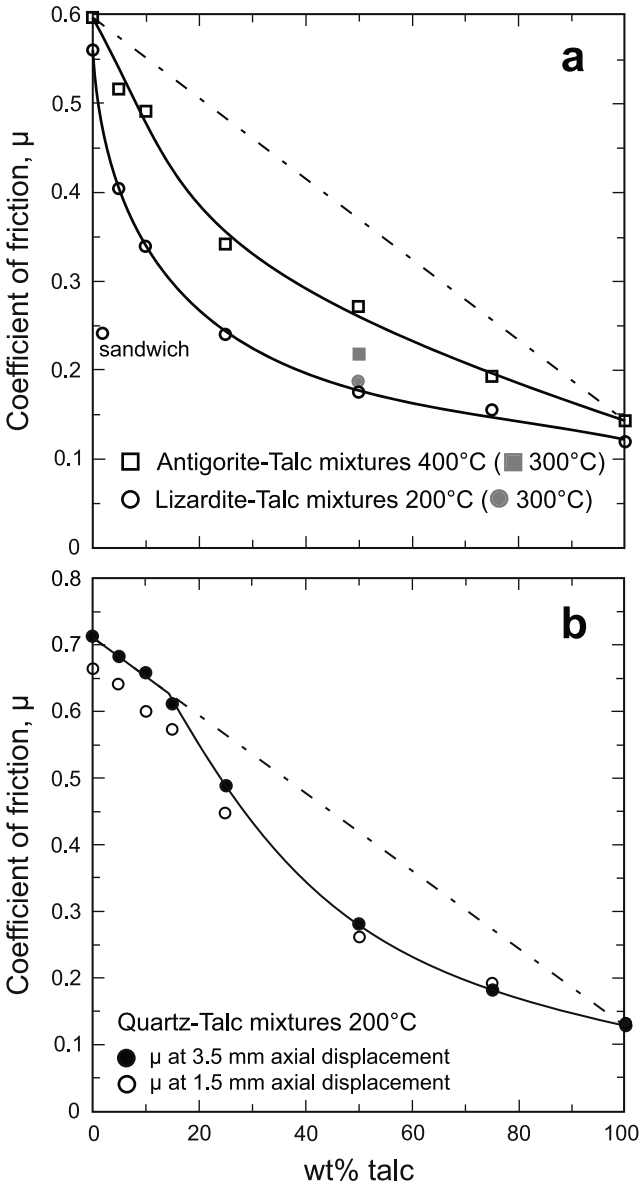

Figure 4. Summary of strength data for mixtures of (a) serpentine and talc and (b) quartz and talc. Because many of the Cu jackets failed before the 3.5 mm end point was reached, the data in Figure 4a represent the strengths at 1.5 mm axial displacement, at the end of the 0.1 μm/s velocity step. None of the Pb jackets used in the quartz-talc series failed prematurely, and the data in Figure 4b provide the final strengths at 3.5 mm axial displacement in addition to those at 1.5 mm. Solid lines were fit visually to the data points for the lizardite-talc (200°C) and antigorite-talc (400°C) series in Figure 4a and the quartz-talc (200°C) series at 3.5 mm axial displacement in Figure 4b. Dashed lines connect the antigorite and talc end-members in Figure 4a and the quartz (3.5 mm) and talc end-members in Figure 4b.

include features such as the noise in the data at 0.01 μm/s. Seal friction is approximately proportional to log(V), and the velocity dependence of seal friction was checked at the beginning of each experiment by means of a velocity step that

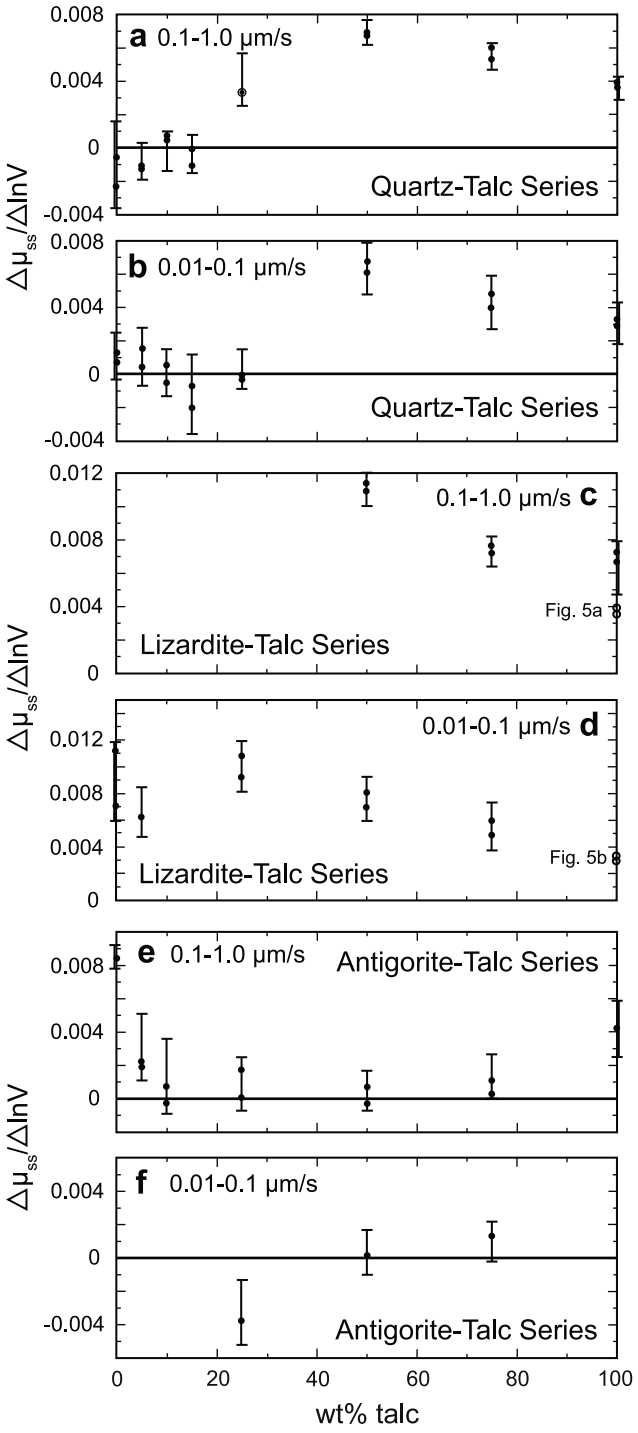

Figure 5. Steady state velocity dependence of frictional strength. A single error bar is drawn for pairs of data points, encompassing the total error estimate for a given pair from the data tables in Appendix A. Dependence at (a) 0.1–1.0 μm/s and (b) 0.01–0.1 μm/s velocity steps for the quartz-talc series and at (c) 0.1–1.0 μm/s and (d) 0.01–0.1 μm/s velocity steps for the lizardite-talc series. The two data points (solid circles) for 100% talc in Figure 5c are from *Moore and Lockner* [2008]. Open circles at 100% talc in Figures 5c and 5d are the data for talc gouge from Figures 5a and 5b, respectively. Dependence at (e) 0.1–1.0 μm/s and (f) 0.01–0.1 μm/s velocity steps for the antigorite-talc series.

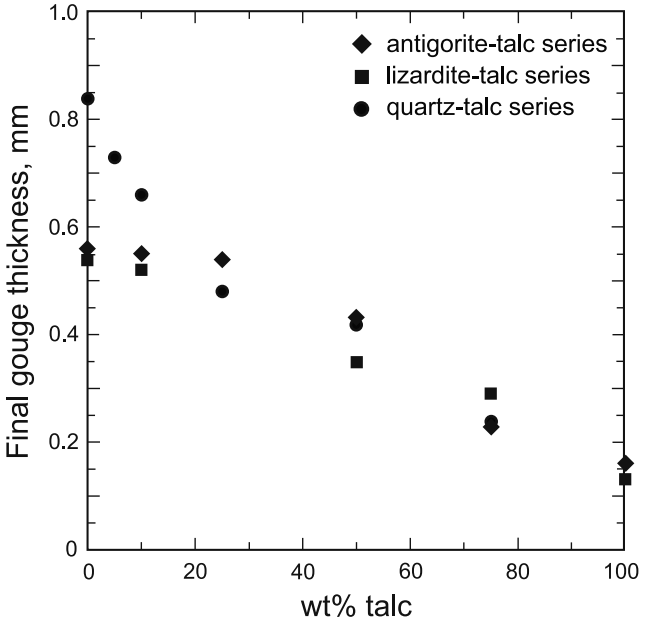

Figure 6. Average thicknesses of gouge layers, measured from thin sections. The two 50:50 talc-serpentine data points are from experiments at 300°C. Data for the end-member lizardite and antigorite gouges were measured on thin sections from previous experiments at 300°C, obtained at the same effective normal stress and velocities used in this study.

was made before the piston reached the sample. For these experiments, a nominal correction of $\Delta\mu_{seal}/\Delta\ln V$ between 0.0007 and 0.0011 to account for the velocity dependence of seal friction was subtracted from the raw data before reporting in the tables in Appendix A.

[22] The quartz-talc series yielded a complete data set (Figures 5a and 5b and Table A1). The quartz-rich samples vary between slightly negative and positive values, whereas all of the values for the more talc-rich samples are positive. The 50% talc sample has the highest value of $\Delta\mu_{ss}/\Delta\ln V$ at both velocity steps.

[23] The lizardite-talc series is all velocity strengthening (Figures 5c and 5d), although data at the faster velocity step are lacking for the lizardite-rich samples. Starting from the talc end-member, $\Delta\mu_{ss}/\Delta\ln V$ generally increases with decreasing talc content of the gouge down to 25–50%. The sandwich sample also is velocity strengthening (Table A2). Some of the velocity data reported by *Moore et al.* [1997] for the lizardite-rich gouge were from experiments that nearly duplicate the conditions of this study. In an experiment at 194°C and 100 MPa σ_N, they measured $\Delta\mu_{ss}/\Delta\ln V = 0.0028$ for a velocity step between 0.1 and 0.32 μm/s and $\Delta\mu_{ss}/\Delta\ln V = -0.0014$ for a step between 0.32 and 1.0 μm/s. These values are consistent with a maximum of $\Delta\mu_{ss}/\Delta\ln V$ at intermediate gouge compositions in Figure 5c.

[24] The antigorite and talc end-members also plot at substantially higher positive values of $\Delta\mu_{ss}/\Delta\ln V$ than the mixtures in Figure 5e. Gouges containing 10–75% talc are transitional between velocity-strengthening and velocity-weakening behaviors. There are few data at the slower step (Figure 5f), and the values change from negative to positive between 25% and 75% talc. The results at 300°C are at higher positive values than those at 400°C (Table A3).

[25] *Tembe et al.* [2010] also found that some mixtures of quartz and clay minerals yielded higher positive values of $\Delta\mu_{ss}/\Delta\ln V$ than either of the end-members. This suggests that the velocity dependence of gouges containing more than one mineral cannot necessarily be predicted from the behavior of the individual constituents. The antigorite-talc series is of particular interest, in that some mixtures may possibly be velocity weakening even though the end-members are velocity strengthening. Both thermally activated rate processes and fluid-rock interactions may influence the velocity dependence of frictional strength (see review by *Paterson and Wong* [2005], and references therein). If so, then differences in the compositions of the minerals at asperity contacts must also be important, particularly at hydrothermal conditions. Additional experiments are warranted, to investigate the roles of fluid and mineral chemistry in the velocity dependence of fault gouge.

3.3. Petrography

[26] A number of the physical features of the gouge samples vary with composition, including the thickness of the sheared gouge layer. As mentioned previously, the thickness of each gouge layer was ≈1 mm prior to the application of confining pressure, although the water contents of the starting gouge pastes probably varied somewhat from sample to sample. The final thicknesses of the compacted and sheared gouge layers, measured from thin sections, are plotted in Figure 6. All reported thickness measurements should be considered upper limits for the values obtaining during the experiments at elevated pressure. Both end-member serpentinite samples had been opened for SEM examination, and the data points for those compositions are from samples tested previously at 300°C, 100 MPa σ_N, and the same range of velocities. The pure quartz gouge (see photomicrograph in Figure 7a) is ≈0.8 mm thick at the end of the experiment, the two serpentinite gouges are ≈0.55 mm thick (e.g., Figure 7b), and the talc gouge (Figure 7c) is only ≈0.15 mm thick. Similarly marked compaction of pure talc gouge was reported by *Moore and Lockner* [2008]. Serpentinite gouges containing ≤25% talc show only a very minor decrease in thickness; at higher talc concentrations, the decrease is roughly linear, although with a scatter of ≈0.1 mm (Figure 6). In contrast to the serpentinite gouges, quartz-gouge thickness decreases with the addition of 5% talc; the quartz-talc trend merges with the serpentinite-talc trends at talc contents ≥25%.

[27] The deformation textures of the end-member sheet-silicate gouges have been described in previous studies [*Moore et al.*, 1997; *Moore and Lockner*, 2004, 2007, 2008]. All three gouges are characterized by localization of shear to very narrow subsidiary traces, generally ≤0.02 mm wide, that either are positioned close to the driving block on one or both sides (referred to as boundary or B shears), or that cross the gouge layer at a small angle to the saw cut surface (R_1 Riedel shears [*Logan et al.*, 1979]) and merge with the B shears at either end (Figures 7b and 7c). Maximum R_1 shear angles in this sample set are 20° for antigorite, 17° for lizardite, and 12° for talc. The samples that

were removed from their jackets for SEM study typically separated along the B and R_1 shears. The shear surfaces are slickensided (Figures 8a and 8b), and the (001) cleavage planes of the phyllosilicates on the shear surfaces are oriented subparallel to the shear plane.

[28] Deformation textures in the quartz gouge correspond to those described previously by *Byerlee et al.* [1978] and others for quartz sheared at high effective stress. Shear in the gouge layer is localized to B and R_1 shears (Figure 7a) that are considerably wider than those in the sheet-silicate

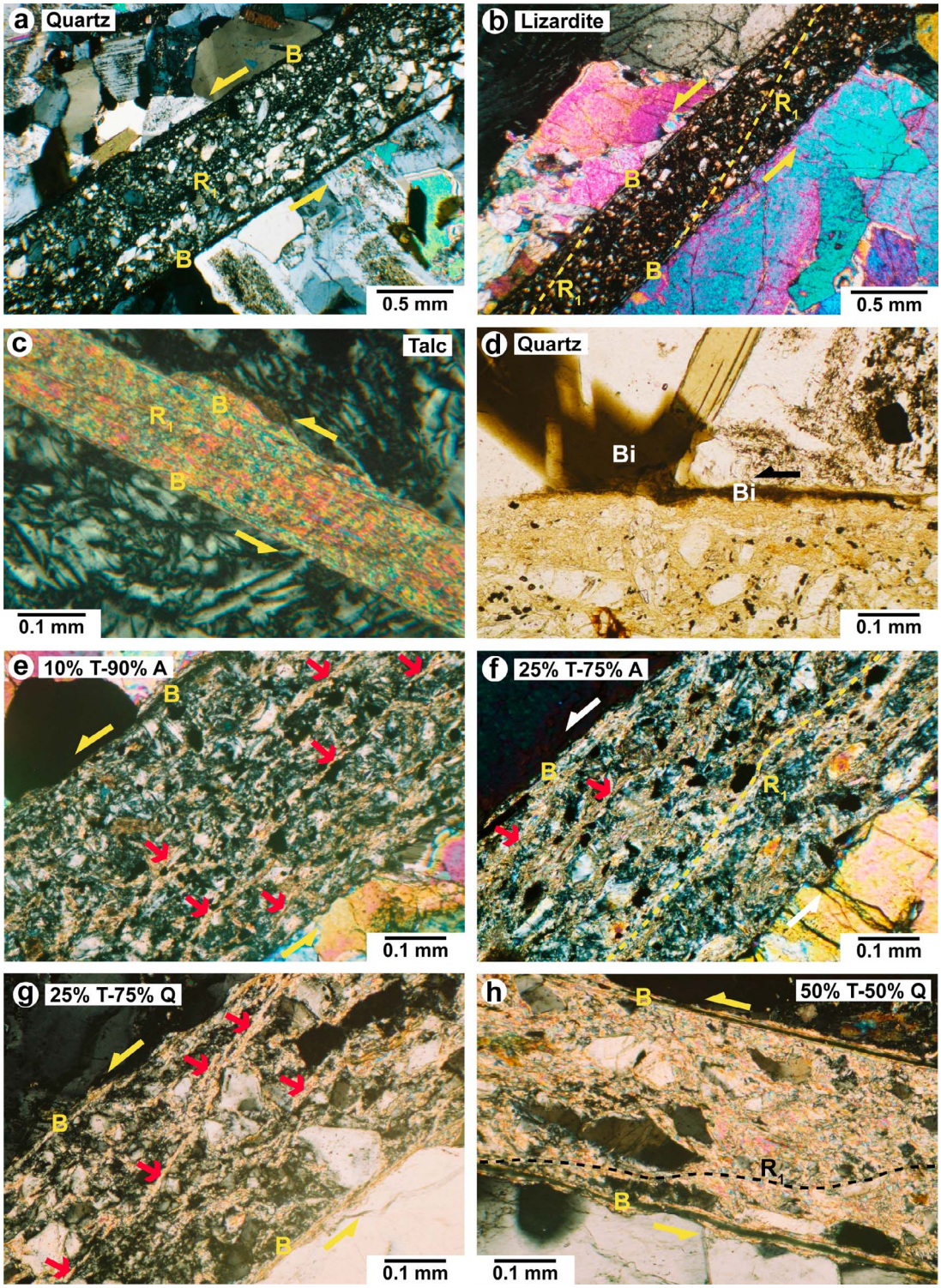

Figure 7

gouges. Boundary shears range in width between about 0.05 and 0.15 mm, and the R_1 shears generally are slightly wider, at 0.1–0.2 mm. Orientations of R_1 shears vary between 8° and 19°. The shears are the site of marked grain-size reduction (Figures 7a and 8c), particularly in the B shears. The shear surfaces in the quartz gouge have a rough, granular texture (Figure 8c) that contrasts with the shiny, slickensided shears in the phyllosilicate gouges (Figures 8a and 8b). Some biotite crystals exposed on the saw cut surfaces of the Westerly granite blocks are smeared out along the boundary shears (Figures 7d and 8d).

[29] Deformation textures in the gouge mixtures differ somewhat from those in the end-member gouges. In the lizardite-talc and antigorite-talc mixtures, throughgoing R_1 traces are largely replaced at low talc concentrations by numerous short segments of R_1 shears that are lined with high-birefringent talc (Figures 7e and 7f). Typical lengths for the short, isolated R_1 segments are in the range 0.15–0.30 mm. Longer segments appear to form by linkage of two or more of the short ones. Both of the serpentinite-rich gouges with 10% talc contain at least one R_1 shear that crosses the entire gouge layer but whose orientation changes several times along its length. One such shear in the 10% talc–90% lizardite gouge has the sequence of orientations relative to the saw cut of 17°, 3°, 9°, 2°, and 10°. That shear widens to as much as 80 μm locally, as talc-lined strands bifurcate around grains of lizardite. Portions of the B shears consist of two parallel strands as much as 70 μm apart. As the talc concentration increases, the number of R_1 shears that cross the gouge layer increases (Figures 7f and 8e). Most of these R_1 shear orientations are ≤11°, and some segments have "Y" or, less commonly, "P" orientations (Figure 7f). At 75% talc content, shears are well defined and narrow (mostly ≤7 μm wide), and their surfaces are largely covered with talc as determined by energy dispersive system (EDS) measurements made during SEM examination.

[30] Overall, deformation textures in the quartz-talc mixtures containing 5–15% talc are the same as those in the pure quartz gouge, with offset localized to well-developed B and R_1 shears that consist of very fine-grained (<10 μm) quartz and talc (Figure 8g). Riedel shear orientations cover the same range as those in the quartz end-member, but their widths decrease slightly with increasing talc content. All of the talc seen in the thin sections appears to be deformed. Talc entrained in B and R_1 shears forms narrow, high-birefringent streaks that are slickensided when viewed with the SEM (Figure 8f), and the platelets are oriented parallel to the shear surfaces (Figure 8g). Talc located away from the shears commonly is oriented at ~20°–30° to the saw cut surface in a P fabric, although a few talc crystals wrap around quartz grains. A few short, talc-lined R_1 shears similar to those found in the serpentinite-talc mixtures first appear in the 10% talc sample.

[31] The quartz-talc mixtures containing 25–75% talc closely resemble the equivalent serpentinite-talc mixtures. The samples with 25% and 50% talc are characterized by short R_1 segments rich in high-birefringent talc, with little ground-up quartz (Figure 7g). A few faint R_1 shears can be traced all the way across the gouge layer, but orientations vary considerably (Figure 7h). Substantial grain-size reduction occurs along well established but narrow (≤0.03 mm wide) B shears, which contain both quartz and talc (Figure 8h). A few R_1 shears similar to those in pure talc are present in the 75% talc sample; they are relatively straight where no large quartz grains are present, but they bend around quartz clasts. The B shears also are deflected as much as 50–60 μm into the gouge layer by quartz clasts. Biotite from the granite driving blocks is incorporated into the boundary shears in the mixtures with ≤25% talc, but not in the samples containing ≥50% talc.

[32] Shear was completely localized along the talc-rich layer in the middle of the sandwich sample (Figure 9). The lighter shaded patches on the shear surfaces in Figure 9a are talc, and the slickensides are more prominent in the talc-rich areas. Figure 9b shows a cross section through one of the gouge halves; the shear direction is perpendicular to the plane of the photo. Along the side that was adjacent to the saw cut, where only lizardite is present, there is no evidence of a B shear, and no R_1 shears are present within the gouge layer. Lizardite comprises most of the thickness of this half layer, and the talc is concentrated on the slickensided shear surface. The strongly planar fabric of the shear extends over an approximately 40 μm thick zone that is separated from the unsheared lizardite gouge by an irregular, 20–30 μm thick transitional zone of compacted lizardite (Figure 9c).

4. Discussion

4.1. Quartz-Talc Mixtures

[33] Very few frictional strength experiments have been conducted on mixtures of quartz and talc. *Van Diggelen et al.* [2009] reported a μ value of ~0.5 for a mixture

Figure 7. Photomicrographs of gouge layers examined in thin section, oriented to show left-lateral offset. All photos except that in Figure 7d were taken under crossed polarizers. (a) Photomicrograph of 100% quartz; general view of gouge layer with boundary (B) shears developed close to each saw cut surface and a relatively wide Riedel (R_1) shear that crosses the gouge layer. Localization of shear is accompanied by considerable grain-size reduction. Photomicrographs of (b) 100% lizardite, 300°C, characterized by narrow B and R_1 shears and relatively undeformed serpentine in the rest of the gouge layer, and (c) 100% talc, 200°C, sheared between serpentinite blocks. The highly compacted gouge layer is very thin compared to the pure quartz and lizardite gouges, but shear nevertheless is localized still further to narrow B and R_1 shears. Photomicrographs of (d) 100% quartz; a biotite (Bi) crystal exposed on the saw cut surface is incorporated in the adjacent B shear; plane-polarized light; (e) 10% talc–90% antigorite, characterized by an "R fabric" consisting of numerous short, talc-lined R_1 traces distributed across the gouge layer; (f) 25% talc–75% antigorite, with several short, talc-lined R_1 traces and a few longer R_1 shears whose orientations vary across the gouge layer; (g) 25% talc–75% quartz, showing the same R fabric as in Figure 7e; and (h) 50% talc–50% quartz, with well-developed B shears and an R_1 shear that is deflected around quartz grains.

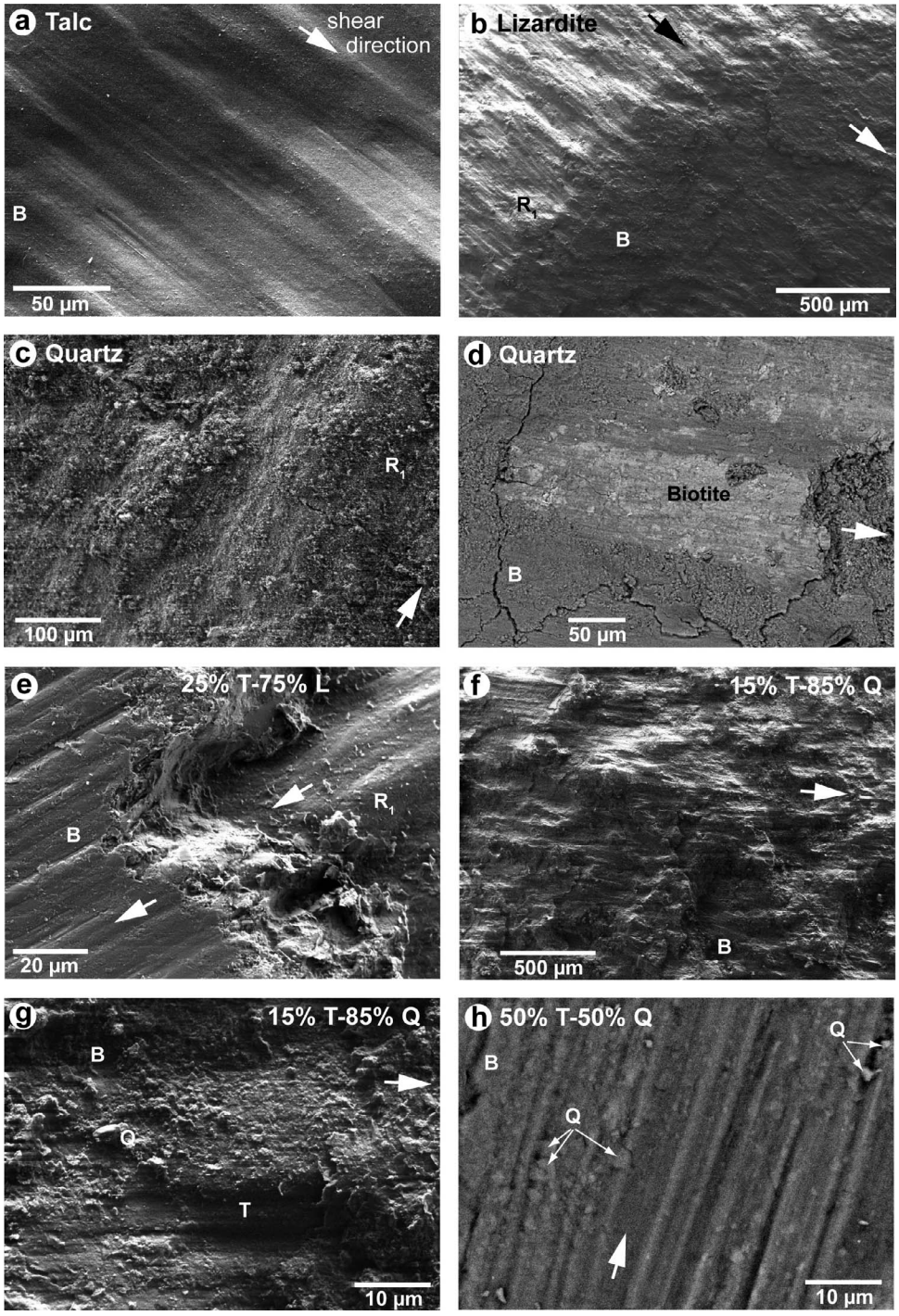

Figure 8. SEM photos of shear surfaces; all except Figures 8d and 8h are secondary electron images. (a) Boundary (B) shear in talc gouge, 200°C. (b) Transition between R_1 and B shears, coincident with the change in brightness of the surface, in 100% lizardite gouge, 200°C. (c) R_1 shear from 100% quartz gouge, 200°C. (d) B shear in 100% quartz gouge layer; bright areas in this backscattered electron (BSE) image are fragments of biotite smeared parallel to the shearing direction. (e) View near the juncture of an R_1 shear with a B shear in gouge with 25% talc and 75% lizardite; deformation is localized along the shears and the gouge between them is relatively undeformed. (f) General view of B shear surface in quartz-rich gouge containing 15% talc; this surface is also very rough but more highly slickensided than that in Figure 8c. (g) High-magnification view of a different location on the B shear in Figure 8f, showing the correspondence between the development of slickensides and the occurrence of talc (T) plates aligned subparallel to the shear surface. (h) BSE image of a B shear in a sample with 50% quartz–50% talc. Small quartz (Q) grains are dispersed in the slickensided, talc-rich shear.

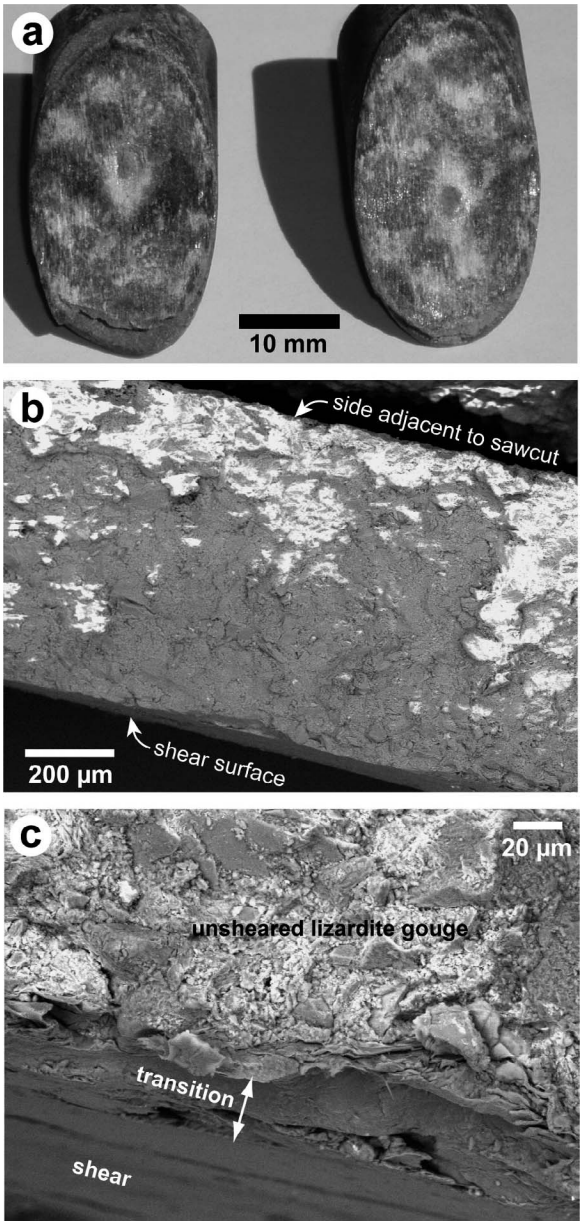

Figure 9. Sandwich sample. (a) When removed from the jacket, the gouge sample separated along a shiny, slickensided planar surface in the middle of the gouge layer where the talc was concentrated. The talc is shaded lighter and the lizardite shaded darker. (b) BSE image of one half of the gouge layer (very bright spots are where the sample became charged under high-voltage (15 kV) conditions). Shearing was concentrated along the surface of the thin band at the bottom. The lizardite gouge above the shear is essentially undeformed. (c) Higher magnification view (BSE) of the sheared side shows the marked contrast between the strongly oriented platy grains in the shear and the adjacent undeformed lizardite gouge. The shear surface is at the lower left corner of the photo.

of 30% talc and 70% quartz in an experiment conducted at 110°C and 50 MPa σ_N (30 MPa fluid pressure). Their value, obtained at a shear strain of ~15, is consistent with the strength of the 25% talc sample (Figures 3a and 4a). *Carpenter et al.* [2009] reported no apparent weakening of quartz when mixed 50:50 with talc. However, their experiments were run on room dry rather than water-saturated samples, which has a considerable effect on talc strength (Figure 10) but none on quartz.

[34] As illustrated in Figure 4b, frictional strength decreases continuously between 0 and 100 wt % talc content, but the rate of decrease varies with gouge composition. An initially linear trend of decreasing strength between the end-member values gives way to higher rates of weakening between 15 and 40–50%, and then to lower rates between ≈50 and 100%. Deformation textures in the gouge layers also vary with gouge composition, and they shed light on the factors controlling the changes in the rate of weakening. At low talc concentrations the numbers and orientations of the subsidiary shears in the gouge samples are essentially the same as in the pure quartz gouge, suggesting that deformation of quartz is the dominant control on the textural development. Talc entrained in the R_1 and B shears is involved in the shearing process, as evidenced by smears of slickensided talc on the shear surfaces (Figure 8g). Short, talc-rich R_1 shear segments first appear in mixtures containing 10% talc.

[35] The onset of marked weakening of the gouge between 15 and 25% talc content corresponds to a striking change in the number and lengths of R_1 shears. The large number of short R_1 shears across the 25% talc sample is clearly controlled by the occurrence of talc within the layer (Figure 7g). In the mixtures, the talc is more or less evenly distributed throughout the gouge, although the spacing of nearest neighbor talc grains will vary over some range. The transition in R_1 shear textures may represent the talc concentration at which a small number of talc grains are sufficiently closely

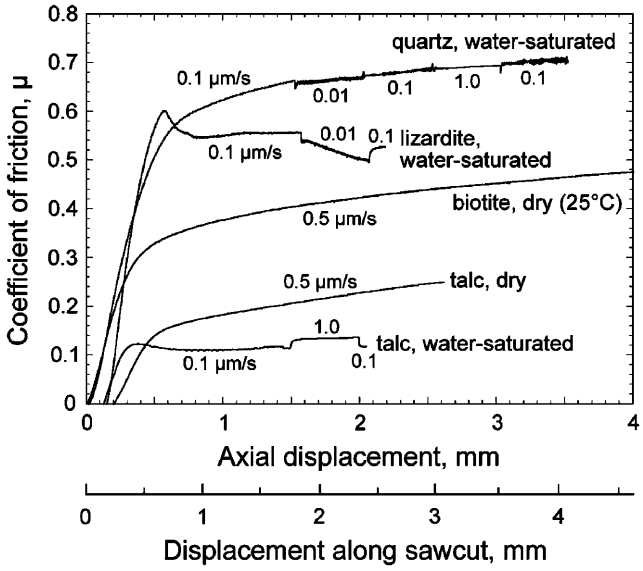

Figure 10. Comparison of the frictional strengths of dry talc [*Moore and Lockner*, 2007] and dry biotite [*Moore and Lockner*, 2004] with the water-saturated strength of talc and lizardite from Figure 2 and strengths of quartz from Figure 3. All experiments were conducted at 100 MPa σ_N, and all except the room temperature biotite experiment were run at 200°C.

spaced that they can link together to form short R_1 shears at multiple sites across the gouge layer. The thickness of the gouge layer must also be a factor. Increasing amounts of talc in a gouge are distributed over a progressively smaller volume, and the 25% talc sample is about half as thick as the pure quartz gouge (Figure 6).

[36] The smears of biotite present in the B shears in quartz-rich samples (Figures 7d and 8d) illustrate a cataclastic process that may aid in the linkage of talc grains to form shears at low talc concentrations. The dry frictional strengths of sheet-structure minerals correlate directly with the strengths of their relatively weak (001) bonds [*Moore and Lockner*, 2004], and the shear strength of dry biotite at 100 MPa effective normal stress is less than that of water-saturated quartz (Figure 10). Because of this, biotite exposed on the saw cut surfaces can be incorporated into the quartz-rich gouge by shear along (001); continued cleaving of the biotite into thinner and thinner platelets produces the streaks. The strength of dry biotite is nearly the same as the strength of the sample containing 25% talc and biotite streaks do not form in the more talc-rich (>25% talc) samples. Dry talc is considerably weaker than dry biotite (Figure 10), and the creation of new cleavage faces, which substantially increases the platy surface area available for frictional sliding, could occur at talc concentrations to nearly 50 wt % (Figure 4b). This cleavage process may be important in talc-bearing faults such as the Zuccale fault on the Isle of Elba, Italy, where *Collettini et al.* [2009b] and *Viti and Collettini* [2009] observed numerous interlayer delaminations of talc lamellae that yielded platelets as thin as 10–30 nm.

[37] Further increases in talc content of the gouge make it progressively easier to localize shear in talc-rich areas. The second change in slope in Figure 4b at ~50% talc may correspond to the point where shear across the gouge layer can be accomplished largely along talc-lined shears, although some fine-grained quartz is a constituent of at least the B shears (Figure 8h). With increasing talc content between 50 and 100% talc, the average length of the R_1 shears increases and an increasing number of them cross the entire gouge layer, although all of the longer R_1 shears bend around quartz grains in the quartz-bearing samples. Because the thickness of the gouge layer decreases with increasing talc content, quartz grains remain a prominent feature of the 75% talc sample, and some of the quartz has been fragmented.

4.2. Serpentinite-Talc Mixtures

[38] *Van Diggelen et al.* [2009] are the only others who have conducted frictional strength tests on serpentine-talc mixtures. They report $\mu \sim 0.2$ for a gouge with 30% talc and 70% serpentinite (serpentine minerals were not identified) tested at 110°C and 50 MPa σ_N. Their results are consistent with the 200°C lizardite-talc series (Figure 4a).

[39] The two serpentinite-talc series (Figure 4a) correspond to the quartz-talc mixtures containing 15–100 wt % talc, both with respect to strength (Figure 4b) and deformation textures (Figure 7). This correspondence suggests that similar deformation processes are operative in the serpentinite-bearing and quartz-bearing gouges over those compositional ranges. However, small quantities of talc are a much more effective weakening agent in serpentinite than in quartz gouge. The reason for this may be the similar platy habits of the talc and the two serpentine minerals. The initial displacement of gouges of layer structure minerals involves compaction, grain size reduction, and in particular rotation of the platy minerals into orientations favorable for the development of subsidiary shears. The peak strengths at around 0.5–1 mm axial displacement in Figure 2 are considered to mark the initiation of shear localization, and the residual strength is reached when the shears are fully developed [e.g., *Moore and Lockner*, 2004]. In the serpentine-rich gouges, the weaker talc platelets may be the first to rotate into the appropriate orientation for shear. The shears then form to as great an extent as possible around these numerous "nucleation" sites. The fact that talc is shearing against another phyllosilicate mineral may also contribute to its ability to localize shear and promote weakening. This would be equivalent to shearing against a smooth rather than a rough surface. Dry talc also is weaker than water-saturated lizardite (Figure 10) and antigorite, and cleaving of talc along (001) likely plays a role in generating talc-lined R_1 shears at low talc concentrations, as it does in the quartz-rich samples. The role, if any, of plastic deformation processes during shear of the phyllosilicate minerals could not be evaluated with the petrographic techniques used in this study.

[40] The short, discontinuous R_1 shears that form in the samples with little talc can be considered as small-scale versions of the sandwich sample, which marks the extreme case of localization. The ~2% talc added to the planar surface in the sandwich sample was sufficient to completely suppress the development of B and R_1 shears, replacing them with a single Y shear. The sample configuration admittedly was such as to optimize the ability of the talc to localize shear, and talc occurring in less favorably oriented planes would likely produce less dramatic reductions in strength. *Niemeijer et al.* [2010] conducted similar experiments in which a talc layer of varying thickness was sandwiched between quartz layers. A ~200 μm thick layer was needed to initiate weakening in their room-dry samples, whereas layers >800 μm thick were as weak as their 100% talc samples.

4.3. Mixing Laws

[41] In recent years, a number of frictional strength investigations have been conducted on mixtures of quartz and various clay minerals under water-saturated conditions at high effective normal stress [e.g., *Takahashi et al.*, 2007; *Crawford et al.*, 2008; *Tembe et al.*, 2010]. Selected results from those studies are presented in Figure 11a along with the talc-quartz series, which corresponds very closely to the montmorillonite-quartz mixtures [*Tembe et al.*, 2010]. Such rock-mechanics experiments commonly have been discussed [e.g., *Takahashi et al.*, 2007; *Crawford et al.*, 2008; *Tembe et al.*, 2010] in terms of the "three-regime" soil mechanics model of *Lupini et al.* [1981], which is based on the bentonite-quartz experiments plotted in Figure 11b. At low and high clay contents the coefficient of friction is essentially the same as that of the quartz and bentonite, respectively, and μ decreases rapidly with increasing clay content at intermediate compositions. This trend in strength was explained [*Lupini et al.*, 1981] in terms of an ideal packing model: At low clay concentrations, the clay-sized bentonite is essentially invisible in the pore spaces and in the clay-rich samples (≥60 wt % bentonite) the large quartz grains are isolated in the clay matrix.

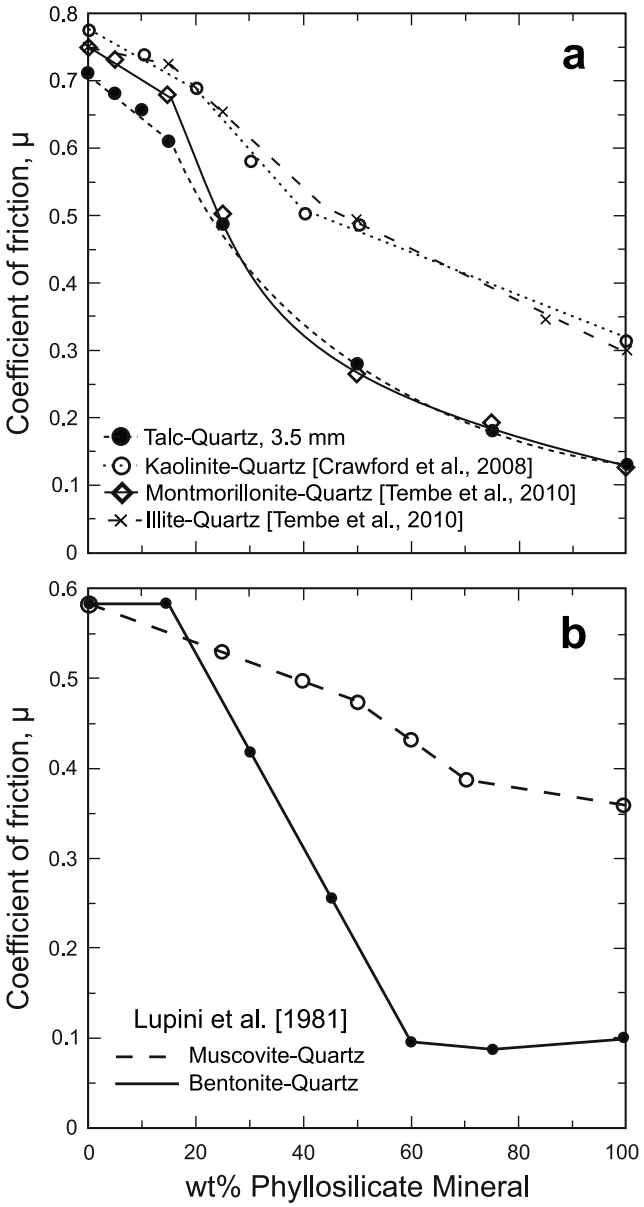

Figure 11. Strength-composition plots for gouge mixtures at low and high σ_N. (a) Comparison of some recent rock mechanics mixing law experiments. The kaolinite-quartz experiments were conducted at 50 MPa effective pressure; data are the values at ~9% shear strain from *Crawford et al.* [2008, Figure 6a]. Montmorillonite-quartz and illite-quartz experiments were run at 40 MPa σ_N; strengths were measured at 8 mm axial displacement [*Tembe et al.*, 2010, Table 1]. (b) Averaged trends from soil mechanics tests at ≤0.35 MPa σ_N, from *Lupini et al.* [1981]. The bentonite-quartz series used sand-sized quartz and largely clay-sized bentonite. For the quartz-muscovite series, mica grains ranged from 30 to 120 μm, overlapping in size with 100–350 μm diameter quartz.

[42] All of the results in Figure 11a differ from the bentonite-quartz series of the model in that strength changes continuously over the entire compositional range, albeit at varying rates. While the transition to a higher rate of strength decrease occurs at similar phyllosilicate concentrations for the four experiments in Figure 11a and the bentonite-quartz mixtures in Figure 11b, this transition occurs at a markedly higher phyllosilicate content of 45% in the montmorillonite-quartz experiments of *Takahashi et al.* [2007]. In addition, both the kaolinite-quartz and illite-quartz series follow nearly linear trends that clearly depart from the three-regime model [*Tembe et al.*, 2010]. However, the quartz-bentonite experiments that form the basis for this model represent a special case with respect to grain-size distributions that is not appropriate for the evaluation of high-pressure experiments. *Lupini et al.* [1981] used nonoverlapping size grading of end-member minerals; the quartz was sand-sized (70–1000 μm diameter), whereas 90% of the bentonite was clay-sized (<2 μm) and all of it was <40 μm in diameter. *Lupini et al.* [1981] also ran experiments on quartz-muscovite mixtures with a grain-size distribution that constitutes one of the numerous listed exceptions to their model. The muscovite consisted of silt-sized to sand-sized particles (≈30–120 μm) that overlapped the size range of the quartz (≈100–350 μm). As illustrated in Figure 8g, similarly overlapping size ranges of quartz and phyllosilicate minerals in a gouge are generated by shear at relatively high σ_N [see also *Crawford et al.*, 2008; *Tembe et al.*, 2010]. The trend of strength versus composition for the muscovite-quartz experiments (Figure 11b) is closely comparable to those for the kaolinite-quartz and illite-quartz mixtures (Figure 11a). In these experiments, at low concentrations the phyllosilicate mineral does not disappear into the void spaces between quartz grains and quartz contributes to the strength of mixtures with high phyllosilicate contents. The increase in the rate of strength reduction in the muscovite-quartz series occurs at ~50% muscovite content, very similar to the transition at 45% montmorillonite content reported by *Takahashi et al.* [2007]. The main differences between the two pairs of experimental results in Figure 11a can be attributed to the different strengths of the phyllosilicate minerals.

[43] A number of other mixing laws have been formulated, and we tested the Voigt and Reuss equations and an area-based mixing law for applicability to our experimental data. These comparisons are summarized in Appendix B. Briefly, we found that a modification of the Reuss model, which was developed to estimate the modulus of elastic materials, successfully reproduces not only the quartz-talc series but also the two serpentine-talc series. The formulation for a two-component mixture is

$$\frac{1}{\mu_{MR}} = \frac{(1 - x_2^p)}{\mu_1} + \frac{x_2^p}{\mu_2}. \quad (1)$$

where μ_{MR} is the coefficient of friction of the mixture (MR, modified Reuss), μ_2 and x_2 are the coefficient of friction and concentration, respectively, of talc, and μ_1 is the coefficient of friction of the second mineral. The modification involves the introduction of the exponent p; the standard Reuss equation is recovered for $p = 1$. Dominance of one mineral over the other is accounted for by changing the value of p. Here, $p < 1$ enhances the influence of the weaker talc while $p > 1$ increases the effect of the stronger mineral. Good fits were achieved using $p = 1$ (standard Reuss equation) for

antigorite-talc mixtures, $p = 0.75$ for lizardite-talc and $p = 1.7$ for quartz-talc (Figures B1–B3). The modified Reuss equation deserves further study for analysis of the frictional strength behavior of polymineralic gouges.

5. Concluding Remarks: Relevance for Fault Zone Weakening

[44] These experiments illustrate the potential importance of even small amounts of talc in reducing the strength of faults, although the degree of weakening as well as the stability of slip may vary with the host rock. Preexisting talc deposits can be cut by younger faults, but more typically the talc is the product of the reaction of Mg-rich rocks such as serpentinite and dolomite with Si-saturated hydrothermal fluids migrating up an active fault. The talc in the faults described in the Introduction was all of syndeformational origin. For example, talc-bearing faults in oceanic lithosphere formed as a result of flow of Si-saturated hydrothermal fluids produced by mafic rock-seawater interaction [*Boschi et al.*, 2006]. Silica-rich fluids released during prograde metamorphism of a subducting slab provide the silica needed to produce serpentine and subsequently talc above the slab-mantle interface [e.g., *Manning*, 1995]. In a similar fashion, talc and calcite have crystallized along the Zuccale low-angle normal fault through the reaction of dolomite with Si-rich fluids generated by contemporaneous magmatic activity [*Collettini et al.*, 2009b; *Viti and Collettini*, 2009].

[45] The initial stages of faulting in these various occurrences may involve relatively diffuse fluid flow along an extensive fracture network. Such flow would eventually lead to the crystallization of minor amounts of talc at numerous sites, in a distribution likely similar to the low-talc gouge mixtures of this study. As these small amounts of weak talc begin to localize shear, a positive feedback mechanism arises causing the Si-charged fluids to become more highly focused along the talc-bearing shears. This in turn concentrates subsequent metasomatic reactions along those shears, further enhancing the weakening. At some point, individual talc-lined shears may become linked, in the manner of the throughgoing R_1 shears with varying orientation seen in the laboratory samples (e.g., Figure 7f). Over time, closely spaced shears may merge into an anastomosing network of talc-rich folia bounding lenses of stronger minerals [e.g., *Collettini et al.*, 2009a]. Such reaction-enhanced weakening processes have been modeled by *Upton and Craw* [2008] for graphite-bearing shear zones.

[46] This study was initiated to address the question of how much talc is needed to significantly weaken a fault, with particular application to the central creeping section of the San Andreas fault. The talc-bearing serpentinite cuttings from the SAFOD drill hole examined by *Moore and Rymer* [2007] also contain the chrysotile variety of serpentine and the Mg-smectite clay saponite, both of which are as weak as talc at the ~3 km depth of the SAFOD drill hole. However, saponite is not stable at temperatures above ~150°C [e.g., *Inoue and Utada*, 1991] and chrysotile becomes substantially stronger at higher temperatures [*Moore et al.*, 1997], leaving talc as a possible mineralogical candidate to explain fault zone weakness at depths greater than 4–5 km. The results of this study demonstrate that if talc is sufficiently localized in its occurrence in a serpentinite-bearing fault, then only a small percentage would be needed, perhaps ≤10% given that the ~2% talc content of the sandwich sample yielded $\mu \approx 0.25$. Detailed petrological investigations and bulk rock analyses of the newly released SAFOD core samples may help to set an upper limit on talc concentrations deeper in the fault, to evaluate the potential of talc for fault zone weakening in the creeping section.

Appendix A: Velocity Dependence of the Coefficient of Friction μ

[47] The velocity dependence of the coefficient of friction μ is given for the quartz-talc series (Table A1), the lizardite-talc series (Table A2), and the antigorite-talc series (Table A3).

Appendix B: Mixing Laws and Bounds

[48] In this section we compare different estimates of shear strength of two-component mixtures to the measured data. We have already discussed how the *Lupini et al.* [1981] three-regime model does not properly represent the serpentine-talc and quartz-talc data as summarized in Figure 4. The dominant feature in the serpentine-talc data is a steadily decreasing strength with increasing talc content. Similar difficulties in applying the Lupini model were noted for quartz-smectite and quartz-kaolinite data by *Tembe et al.* [2010]. Two commonly used mixing laws were developed to estimate the modulus of elastic materials. They are the Voigt upper bound

$$M_V = \sum_i x_i M_i \tag{B1}$$

and the Reuss lower bound

$$\frac{1}{M_R} = \sum_i \frac{x_i}{M_i}, \tag{B2}$$

which have been applied to a variety of physical properties including body wave speed, fluid and magnetic permeability, and electrical conductivity. For elastic modulus, the Voigt upper bound is obtained assuming that all constituents undergo identical strain. Similarly, the Reuss lower bound is obtained by assuming that all constituents are subjected to identical stress. For electrical circuits, the two bounds correspond to resistive elements connected in series (equal current) and in parallel (equal voltage), respectively.

[49] We can apply the Voigt and Reuss formulations to estimate the equivalent coefficient of friction for two-component mixtures according to

$$\mu_V = x_1\mu_1 + x_2\mu_2 = (1 - x_2)\mu_1 + x_2\mu_2 \tag{B3}$$

$$\frac{1}{\mu_R} = \frac{x_1}{\mu_1} + \frac{x_2}{\mu_2} = \frac{(1 - x_2)}{\mu_1} + \frac{x_2}{\mu_2}. \tag{B4}$$

[50] Here, μ_V and μ_R are the coefficients of friction of the mixture determined using the Voigt and Reuss formulations, respectively; μ_2 and x_2 are the coefficient of friction and concentration of talc, respectively, and μ_1 and x_1 the coef-

Table A1. Quartz-Talc Series

Sample	Axial Velocity Step (μm/s)	$\Delta\mu_{ss}/\Delta\ln V$ Value	Minimum $\Delta\mu_{ss}/\Delta\ln V$	Maximum $\Delta\mu_{ss}/\Delta\ln V$
0 wt % Talc	0.01–0.1	0.0013	0.0	0.0025
	0.01–0.1	0.0007	−0.0003	0.0018
	0.1–1.0	−0.0006	−0.0024	0.0010
	0.1–1.0	−0.0023	−0.0036	0.0016
5% Talc	0.01–0.1	0.0016	−0.0001	0.0028
	0.01–0.1	0.0004	−0.0007	0.0019
	0.1–1.0	−0.0011	−0.0017	0.0003
	0.1–1.0	−0.0013	−0.0019	−0.0006
10% Talc	0.01–0.1	0.0005	−0.0003	0.0015
	0.01–0.1	−0.0005	−0.0013	0.0006
	0.1–1.0	0.0004	−0.0014	0.0010
	0.1–1.0	0.0008	0.0004	0.0010
15% Talc	0.01–0.1	−0.0020	−0.0036	−0.0002
	0.01–0.1	−0.0007	−0.0014	0.0012
	0.1–1.0	−0.0001	−0.0006	0.0008
	0.1–1.0	−0.0011	−0.0015	−0.0007
25% Talc	0.01–0.1	−0.0003	−0.0006	0.0015
	0.01–0.1	−0.0001	−0.0009	0.0011
	0.1–1.0	0.0033	0.0026	0.0039
	0.1–1.0	0.0033	0.0025	0.0057
50% Talc	0.01–0.1	0.0068	0.0058	0.0079
	0.01–0.1	0.0061	0.0048	0.0074
	0.1–1.0	0.0067	0.0065	0.0076
	0.1–1.0	0.0069	0.0062	0.0077
75% Talc	0.01–0.1	0.0048	0.0036	0.0059
	0.01–0.1	0.0040	0.0027	0.0053
	0.1–1.0	0.0060	0.0056	0.0063
	0.1–1.0	0.0053	0.0047	0.0063
100% Talc	0.01–0.1	0.0033	0.0021	0.0043
	0.01–0.1	0.0029	0.0018	0.0043
	0.1–1.0	0.0039	0.0035	0.0042
	0.1–1.0	0.0036	0.0029	0.0043

Table A3. Antigorite-Talc Series

Sample	Axial Velocity Step (μm/s)	$\Delta\mu_{ss}/\Delta\ln V$ Value	Minimum $\Delta\mu_{ss}/\Delta\ln V$	Maximum $\Delta\mu_{ss}/\Delta\ln V$
0 wt % Talc	0.1–1.0	0.0084	0.0078	0.0092
5% Talc	0.1–1.0	0.0023	0.0015	0.0051
	0.1–1.0	0.0019	0.0011	0.0027
10% Talc	0.1–1.0	0.0007	−0.0001	0.0036
	0.1–1.0	−0.0003	−0.0009	0.0003
25% Talc	0.1–1.0	0.0017	0.0011	0.0025
	0.1–1.0	0.0001	−0.0007	0.0009
	0.01–0.1	−0.0038	−0.0052	−0.0013
50% Talc	0.1–1.0	0.0007	0.0003	0.0017
	0.1–1.0	−0.0003	−0.0007	0.0001
	0.01–0.1	0.0001	−0.0010	0.0017
75% Talc	0.1–1.0	0.0011	0.0004	0.0027
	0.1–1.0	0.0003	−0.0004	0.0012
	0.01–0.1	0.0013	−0.0002	0.0022
100% Talc	0.1–1.0	0.0042	0.0025	0.0059
50% Talc, 300°C	0.1–1.0	0.0066	0.0041	0.0071
	0.1–1.0	0.0063	0.0060	0.0077
	0.01–0.1	0.0038	0.0027	0.0046

ficients of friction and concentrations of the second mineral, respectively. Voigt and Reuss bounds are compared to antigorite-talc friction data in Figure B1. In this case, the observed strength data closely follow the Reuss bound. If we use the analogy for equivalent elastic modulus, the close conformity to the Reuss bound suggests that under steady flow conditions the antigorite and talc constituents tend to deform under uniform local stress conditions.

[51] A simple fault surface area-based mixing law model was brought to our attention by N. Beeler (personal communication, 2009). In this case, consider a narrow slip surface bounded above and below by the constituent minerals m_1 and m_2. Three possible configurations exist for contacts on the slip surface: m_1-m_1, m_2-m_2, and m_1-m_2. The m_1-m_1 contacts have strength μ_1 and the m_2-m_2 contacts have

Table A2. Lizardite-Talc Series

Sample	Axial Velocity Step (μm/s)	$\Delta\mu_{ss}/\Delta\ln V$ Value	Minimum $\Delta\mu_{ss}/\Delta\ln V$	Maximum $\Delta\mu_{ss}/\Delta\ln V$
0 wt % Talc	0.01–0.1	0.0070	0.0059	0.0075
	0.01–0.1	0.0111	0.0101	0.0118
5% Talc	0.01–0.1	0.0061	0.0047	0.0084
25% Talc	0.01–0.1	0.0108	0.0096	0.0119
	0.01–0.1	0.0092	0.0081	0.0113
50% Talc	0.01–0.1	0.0080	0.0070	0.0092
	0.01–0.1	0.0069	0.0059	0.0083
	0.1–1.0	0.0109	0.0100	0.0114
	0.1–1.0	0.0114	0.0107	0.0120
75% Talc	0.01–0.1	0.0059	0.0043	0.0073
	0.01–0.1	0.0049	0.0037	0.0060
	0.1–1.0	0.0071	0.0064	0.0077
	0.1–1.0	0.0076	0.0067	0.0082
100% Talc	0.1–1.0	0.0066	0.0047	0.0078
	0.1–1.0	0.0072	0.0065	0.0079
Sandwich, ≈2%	0.01–0.1	0.0143	0.0136	0.0148
	0.01–0.1	0.0134	0.0119	0.0141
50% Talc, 300°C	0.01–0.1	0.0111	0.0100	0.0122
	0.01–0.1	0.0066	0.0054	0.0078
	0.1–1.0	0.0083	0.0060	0.0094
	0.1–1.0	0.0088	0.0083	0.0097

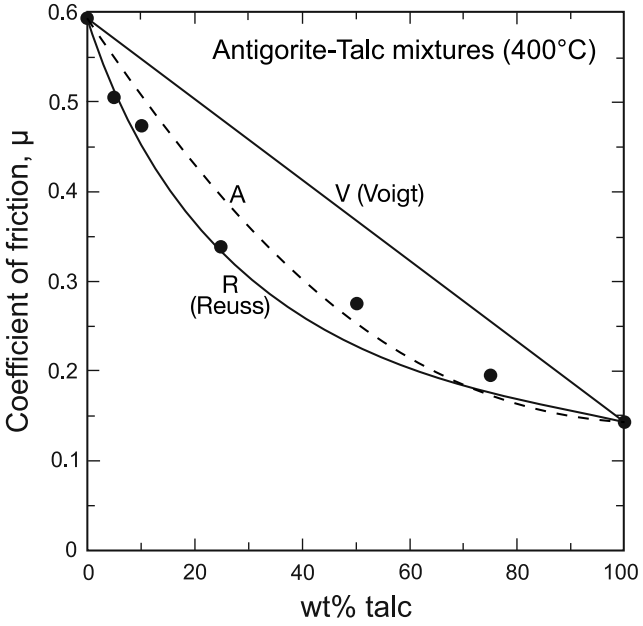

Figure B1. Coefficient of friction (μ) for antigorite-talc mixtures at 400°C and 1.5 mm axial shortening (1.73 mm fault-parallel slip). Solid circles are observed data. Model approximations are labeled V for Voigt bound (equation (B3)), R for Reuss bound (equation (B4)) and A for equivalent area model (equation (B5)) results.

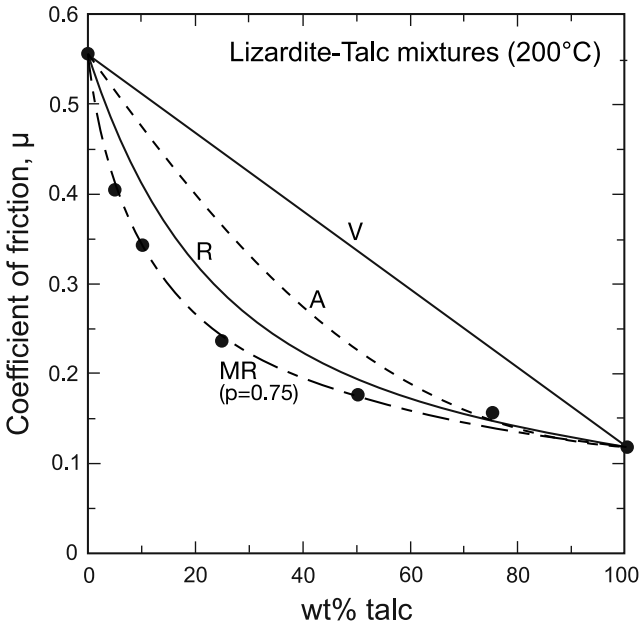

Figure B2. Coefficient of friction for lizardite-talc mixtures at 200°C and 1.5 mm axial shortening. Symbols are the same as in Figure B1. In addition, results from a modified Reuss (MR) model are shown (equation (B6)) with parameter $p = 0.75$. Values of p less than unity enhance the weakening effect of the talc.

strength μ_2. However, it is likely that the m_1-m_2 contacts have the strength of the weaker (μ_2) constituent. If the area A_1 of component m_1 on the slip surface is proportional to the concentration x_1 of that component, then the proportion of m_1-m_1 surface area is x_1^2. Since, in this model, this is the only contact configuration that has strength μ_1, the remainder of the surface area $(1 - x_1^2)$ has strength μ_2 and the equivalent strength becomes

$$\mu_A = x_1^2\mu_1 + \left(1 - x_1^2\right)\mu_2 = (1 - x_2)^2\mu_1 + \left(1 - (1 - x_2)^2\right)\mu_2. \tag{B5}$$

[52] This area-based equivalent strength model is plotted for the antigorite-talc data in Figure B1. The model captures the general shape of the observed strength versus weight fraction data but under predicts the enhanced weakening effect of talc below concentrations of 45%.

[53] The Voigt, Reuss, and area-based models are compared to the lizardite-talc data in Figure B2. The simple Voigt averaging completely misses the enhanced weakening effect of talc in low concentrations. This weakening is so pronounced for the lizardite-talc system that the Reuss and area-based equivalent strength models also overestimate the observed strength. However, the enhanced weakening effect of talc can be modeled by a simple modification of the Reuss formulation:

$$\frac{1}{\mu_{MR}} = \frac{\left(1 - x_2^p\right)}{\mu_1} + \frac{x_2^p}{\mu_2}. \tag{B6}$$

[54] In this case, dominance of either mineral constituent can be included by changing the exponent p. Decreasing p enhances the influence of the weaker talc mineral while increasing p enhances the effect of the stronger mineral. The standard Reuss equation (B4) is recovered for $p = 1$. This modified Reuss model is plotted in Figure B2 using $p = 0.75$. The additional level of complexity provides a good fit to the observed data.

[55] As a final example, the four model fits are compared to the quartz-talc data in Figure B3. In this case, Voigt averaging provides reasonable agreement for talc concentrations below about 15%. The Reuss model consistently underestimates the observed strength while the area-based model provides reasonable agreement for talc concentrations above ~30%. In the modified Reuss model, the exponent p is a free parameter. Choosing a value of $p = 1.7$ provides a remarkably good fit to the observed data. Because p is greater than one, the strengthening effect of quartz is enhanced. While this exponent was chosen to match the strength characteristics at low talc concentration, it also follows the observed strength curve for high talc concentration as well. The quartz-talc data actually remain slightly above the Voigt curve for talc concentrations less than 15%. While the deviation from the Voigt curve is small and is probably within the experimental uncertainty, the modified Reuss model actually shows a similar trend in Figure B3 in that it plots above the Voigt bound for low talc concentrations. *Tembe et al.* [2010] reported a similar and more pronounced quartz strengthening effect for their quartz-illite-montmorillonite mixture. It is not clear what the physical basis is for the good performance of equation (B6) in matching the talc friction data. This is a topic that warrants further consideration.

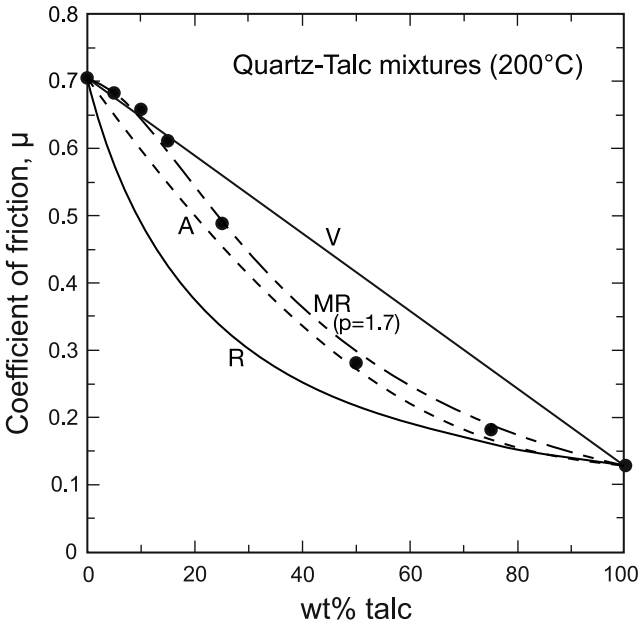

Figure B3. Coefficient of friction for quartz-talc mixtures at 200°C and 3.5 mm axial shortening (4.03 mm fault-parallel slip). Symbols are the same as in Figure B1. In addition, MR results are shown (equation (B6)) with parameter $p = 1.7$. Values of p greater than unity enhance the strengthening effect of the quartz.

[56] **Acknowledgments.** We thank B. Kilgore and T.-f. Wong for their careful reviews of an earlier version of the manuscript and C. Spiers, an unknown reviewer, and Associate Editor D. Faulkner for their helpful suggestions for improving the submitted manuscript. R. Oscarson provided help with the SEM work.

References

Bebout, G. E., and M. D. Barton (2002), Tectonic and metasomatic mixing in a high-T, subduction-zone mélange: Insights into the geochemical evolution of the slab-mantle interface, *Chem. Geol.*, *187*, 79–106, doi:10.1016/S0009-2541(02)00019-0.

Boschi, C., G. L. Früh-Green, and J. Escartin (2006), Occurrence and significance of serpentinite-hosted, talc- and amphibole-rich fault rocks in modern oceanic settings and ophiolite complexes: An overview, *Ofioliti*, *31*, 129–140.

Byerlee, J., V. Mjachkin, R. Summers, and O. Voevoda (1978), Structures developed in fault gouge during stable sliding and stick-slip, *Tectonophysics*, *44*, 161–171, doi:10.1016/0040-1951(78)90068-9.

Carpenter, B. M., C. Marone, and D. M. Saffer (2009), Frictional behavior of materials in the 3D SAFOD volume, *Geophys. Res. Lett.*, *36*, L05302, doi:10.1029/2008GL036660.

Chernosky, J. V., Jr., H. W. Day, and L. J. Caruso (1985), Equilibria in the system MgO-SiO_2-H_2O: Experimental determination of the stability of Mg-anthophyllite, *Am. Mineral.*, *70*, 223–236.

Chester, F. M., and N. G. Higgs (1992), Multimechanism friction constitutive model for ultrafine quartz gouge at hypocentral conditions, *J. Geophys. Res.*, *97*, 1859–1870, doi:10.1029/91JB02349.

Collettini, C., A. Niemeijer, C. Viti, and C. Marone (2009a), Fault zone fabric and fault weakness, *Nature*, *462*, 907–910, doi:10.1038/nature08585.

Collettini, C., C. Viti, S. A. F. Smith, and R. E. Holdsworth (2009b), Development of interconnected talc networks and weakening of continental low-angle normal faults, *Geology*, *37*, 567–570, doi:10.1130/G25645A.1.

Crawford, B. R., D. R. Faulkner, and E. H. Rutter (2008), Strength, porosity, and permeability development during hydrostatic and shear loading of synthetic quartz-clay fault gouge, *J. Geophys. Res.*, *113*, B03207, doi:10.1029/2006JB004634.

Higgs, N. G. (1981), Mechanical properties of ultrafine quartz, chlorite, and bentonite in environments appropriate to upper-crustal earthquakes, Ph. D. dissertation, 267 pp., Texas A&M Univ., College Station, Tex.

Inoue, A., and M. Utada (1991), Smectite-to-chlorite transformation in thermally metamorphosed volcaniclastic rocks in the Kamikita area, northern Honshu, Japan, *Am. Mineral.*, *76*, 628–640.

Jenkins, D. M., T. J. B. Holland, and A. K. Clare (1991), Experimental determination of the pressure-temperature stability field and thermochemical properties of synthetic tremolite, *Am. Mineral.*, *76*, 458–469.

King, R. L., M. J. Kohn, and J. M. Eiler (2003), Constraints on the petrologic structure of the subduction slab-mantle interface from Franciscan Complex exotic ultramafic blocks, *Geol. Soc. Am. Bull.*, *115*, 1097–1109, doi:10.1130/B25255.1.

Logan, J. M., M. Friedman, N. Higgs, C. Dengo, and T. Shimamoto (1979), Experimental studies of simulated gouge and their application to studies of natural fault zones, *U. S. Geol. Surv. Open File Rep.*, *79-1239*, 305–343.

Lupini, J. F., A. E. Skinner, and P. R. Vaughan (1981), The drained residual strength of cohesive soils, *Geotechnique*, *31*, 181–213, doi:10.1680/geot.1981.31.2.181.

Manning, C. E. (1995), Phase-equilibrium controls on SiO_2 metasomatism by aqueous fluid in subduction zones: Reaction at constant pressure and temperature, *Int. Geol. Rev.*, *37*, 1074–1093, doi:10.1080/00206819509465440.

Moore, D. E., and D. A. Lockner (2004), Crystallographic controls on the frictional behavior of dry and water-saturated sheet structure minerals, *J. Geophys. Res.*, *109*, B03401, doi:10.1029/2003JB002582.

Moore, D. E., and D. A. Lockner (2007), Comparative deformation behavior of minerals in serpentinized ultramafic rock: Application to the slab-mantle interface in subduction zones, *Int. Geol. Rev.*, *49*, 401–415, doi:10.2747/0020-6814.49.5.401.

Moore, D. E., and D. A. Lockner (2008), Talc friction in the temperature range 25°C–400°C: Relevance for fault-zone weakening, *Tectonophysics*, *449*, 120–132, doi:10.1016/j.tecto.2007.11.039.

Moore, D. E., and M. J. Rymer (2007), Talc-bearing serpentinite and the creeping section of the San Andreas fault, *Nature*, *448*, 795–797, doi:10.1038/nature06064.

Moore, D. E., D. A. Lockner, R. Summers, J. D. Byerlee, and S. Ma (1996), Sample characterizations and strength measurements of serpentinite gouges, *U. S. Geol. Surv. Open File Rep.*, *96-702*, 88 pp.

Moore, D. E., D. A. Lockner, S. Ma, R. Summers, and J. D. Byerlee (1997), Strengths of serpentinite gouges at elevated temperatures, *J. Geophys. Res.*, *102*, 14,787–14,801, doi:10.1029/97JB00995.

Morrow, C. A., D. E. Moore, and D. Lockner (2000), The effect of mineral bond strength and adsorbed water on fault gouge frictional strength, *Geophys. Res. Lett.*, *27*, 815–818, doi:10.1029/1999GL008401.

Niemeijer, A., C. Marone, and D. Elsworth (2010), Fabric induced weakness of tectonic faults, *Geophys. Res. Lett.*, *37*, L03304, doi:10.1029/2009GL041689.

Paterson, M. S., and T.-F. Wong (2005), *Experimental Rock Deformation: The Brittle Field*, 2nd ed., 347 pp., Springer, New York.

Pawley, A. R., and B. J. Wood (1995), The high-pressure stability of talc and 10 Å phase: Potential storage sites for H_2O in subduction zones, *Am. Mineral.*, *80*, 998–1003.

Peacock, S. M. (1987), Serpentinization and infiltration metasomatism in the Trinity peridotite, Klamath province, northern California: Implications for subduction zones, *Contrib. Mineral. Petrol.*, *95*, 55–70, doi:10.1007/BF00518030.

Scott, D. R., D. A. Lockner, J. D. Byerlee, and C. G. Sammis (1994), Triaxial testing of Lopez fault gouge at 150 MPa mean effective stress, *Pure Appl. Geophys.*, *142*, 749–775, doi:10.1007/BF00876063.

Takahashi, M., K. Mizoguchi, K. Kitamura, and K. Masuda (2007), Effects of clay content on the frictional strength and fluid transport property of faults, *J. Geophys. Res.*, *112*, B08206, doi:10.1029/2006JB004678.

Tembe, S., D. A. Lockner, and T.-F. Wong (2010), Effect of clay content and mineralogy on frictional sliding behavior of simulated gouges: Binary and ternary mixtures of quartz, illite, and montmorillonite, *J. Geophys. Res.*, *115*, B03416, doi:10.1029/2009JB006383.

Upton, P., and D. Craw (2008), Modeling of the role of graphite in development of a mineralized midcrustal shear zone, Macraes mine, New Zealand, *Earth Planet. Sci. Lett.*, *266*, 245–255, doi:10.1016/j.epsl.2007.10.048.

Van Diggelen, E., J. H. De Bresser, and C. Spiers (2009), The effect of phyllosilicates and matrix on fault strength: Implications for the San Andreas fault zone, *Eos Trans AGU*, *90*, Fall Meet. Suppl., Abstract T53C–1601.

Viti, C., and C. Collettini (2009), Growth and deformation mechanisms of talc along a natural fault: A micro/nanostructural investigation, *Contrib. Mineral. Petrol.*, *158*, 529–542, doi:10.1007/s00410-009-0395-4.

D. A. Lockner and D. E. Moore, U.S. Geological Survey, 345 Middlefield Rd., MS977, Menlo Park, CA 94025, USA. (dmoore@usgs.gov)